

## SPITZER OBSERVATIONS OF THE DUSTY WARPED DISK OF CENTAURUS A

ALICE C. QUILLEN

Department of Physics and Astronomy, University of Rochester, Rochester, NY 14627

MAIRI H. BROOKES, JOCELYN KEENE, DANIEL STERN, CHARLES R. LAWRENCE, MICHAEL W. WERNER  
 Jet Propulsion Laboratory, 4800 Oak Grove Drive, Pasadena, CA 91109

*Draft version October 19, 2018*

### ABSTRACT

*Spitzer* mid-infrared images of the dusty warped disk in the galaxy Centaurus A show a parallelogram-shaped structure. We successfully model the observed mid-infrared morphology by integrating the light from an emitting, thin, and warped disk, similar to that inferred from previous kinematic studies. The models with the best match to the morphology lack dust emission within the inner 0.1 to 0.8 kpc, suggesting that energetic processes near the nucleus have disturbed the inner molecular disk, creating a gap in the molecular gas distribution.

*Subject headings:* galaxies: structure – galaxies: ISM – galaxies: individual (NGC 5128) – galaxies: peculiar

### 1. INTRODUCTION

Centaurus A (NGC 5128) is the nearest of all the giant radio galaxies. Because of the disk of gas and dust in its central regions, Centaurus A is suspected to be the product of a merger of a small gas rich spiral galaxy with a larger elliptical galaxy (Baade & Minkowski 1954). Numerical simulations of such mergers predict large shell-like features (Hernquist & Quinn 1988) that have been observed in Centaurus A over a large range of radii (Malin et al. 1983; Peng et al. 2002). Some contain atomic and molecular gas, implying that they were formed from material stripped from a galaxy relatively recently, fewer than a few galactic rotation periods ago (Schiminovich et al. 1994; Charmandaris et al. 2000). Tidal features associated with this debris have also been identified, supporting the relatively short (few times  $10^8$  years) estimated timescale since the merger took place (Peng et al. 2002).

In its central regions, NGC 5128 exhibits a well recognized, optically-dark band of absorption across its nucleus. This dusty disk was first modeled as a transient warped structure by Tubbs (1980). Bland (1986), Bland et al. (1987), Quillen et al. (1992), and Nicholson et al. (1992) found that the kinematics of the ionized and molecular gas are well modeled by a warped disk composed of a series of inclined connected rings undergoing circular motion (as also explored for other galaxies with peculiar morphology by Steiman-Cameron et al. 1992). The model explored by Quillen, Graham & Frogel (1993) modified the kinematic model by Quillen et al. (1992) to fit the morphology of the absorptive, dusty disk seen in near-infrared images and proposed a timescale of about 200 million years since the core of an infalling spiral galaxy reached and merged with the elliptical galaxy nucleus. An initially flat disk, misaligned with the galaxy principal sym-

metry axis, becomes increasingly corrugated as a function of time. The short timescale estimated since the merger in NGC 5128 is approximately consistent with the timescale suggested by the presence of tidal debris and by the shell-like features containing atomic hydrogen (Schiminovich et al. 1994; Peng et al. 2002) and molecular gas (Charmandaris et al. 2000). An alternative model accounting for the warped disk is the polar ring model by Sparke (1996), consistent with the polar orbit of the disk implied by the galaxy isophotes in the outer galaxy (Malin et al. 1983; Haynes et al. 1983; Peng et al. 2002) but requiring a longer timescale to account for the twist of the warp.

More recent observations of the central region include submillimeter imaging with the Submillimeter Common User Bolometer Array (SCUBA) and mid-IR imaging with the Infrared Camera (ISOCAM) on the *Infrared Space Observatory (ISO)* satellite (Mirabel 1999; Leeuw et al. 2002). At these wavelengths, the dusty disk is seen in emission rather than absorption. At 100–200 pc from the nucleus the galaxy contains a molecular circumnuclear disk that has been studied in molecular line emission (Israel et al. 1990, 1991) and resolved in Pa $\alpha$  emission (Schreier et al. 1996; Marconi et al. 2001). For a recent summary of the wealth of observational studies carried out on this peculiar and active nearby galaxy, see the comprehensive review by Israel (1998). Based on the discussion by Israel (1998), we adopt a distance to Centaurus A of 3.4 Mpc. At this distance 1' on the sky corresponds to  $\sim 1$  kpc.

In this manuscript we focus on the geometry of the dusty disk in Centaurus A as seen from *Spitzer* Infrared Array Camera (IRAC) images. These images resolve the structure of the disk more clearly than previous observations and also show the disk out to larger radii. They provide us with an opportunity to study the geometry of the warped disk in much higher detail than previously possible. Observations are described in § 2. Our geometric model is described in § 3. A discussion and summary follow in § 4.

### 2. OBSERVATIONS

Electronic address: aquillen@pas.rochester.edu  
 Electronic address: Mairi.H.Brookes@jpl.nasa.gov  
 Electronic address: jkeene@caltech.edu  
 Electronic address: charles.lawrence@jpl.nasa.gov  
 Electronic address: Michael.W.Werner@jpl.nasa.gov  
 Electronic address: stern@zwolfkinder.jpl.nasa.gov

Figures 1 and 2 present images of NGC 5128 taken on 2004 February 10 in the 3.6, 4.5, 5.8 and 8.0  $\mu\text{m}$  broadband filters (channels 1-4) of the *Spitzer* Infrared Array Camera (IRAC; Fazio et al. 2004). In each filter, *fixed cluster* observing mode was used for these observations to produce a map of  $5 \times 6$  points, at which five dithered exposures were taken. The exposure time per frame was 12 s. Additional shorter exposure, 0.4 s frames, were also taken to correct for possible saturation in the longer exposure frames. The coverage of the map at each position on the sky varies between three and ten frames, with an average coverage of six frames, corresponding to an exposure time of 72 s.

Before mosaicing, the *basic calibrated data* (BCD) frames were corrected for artifacts using the IRAC artifact mitigation code (excluding the pulldown correction) available from the *Spitzer* Science Center contributed software pages<sup>1</sup>. The final mosaiced images were produced from the dithered frames by applying the *MOPEX* software<sup>2</sup> to the corrected BCD frames.

Here we focus on the central  $5' \times 5'$  region in the final mosaics. The mosaiced images provide a plate scale with  $1.^{\circ}2$  pixels; FWHMs of the point spread functions are  $1.7$ ,  $1.7$ ,  $1.9$ ,  $2.^{\circ}0$  in channels 1-4, respectively. The rms noise levels in these images are  $0.025$ ,  $0.024$ ,  $0.070$ , and  $0.060 \text{ MJy sr}^{-1}$  in channels 1-4, respectively. The above sensitivities agree with the predictions of the *SENS-PET* sensitivity estimator in longer wavelengths channels. The  $3.6 \mu\text{m}$  channel contains emission from the stellar component of the galaxy that extends over a large portion of the field of view. This makes the  $3.6 \mu\text{m}$  image about half as sensitive as the *SENS-PET* prediction for the dust emission.

The IRAC images presented here are deeper than previous ISOCAM images (Mirabel (1999)), and have higher angular resolution than previous submillimeter images ((Mirabel 1999; Leeuw et al. 2002)). In the inner few arcminutes, the IRAC images exhibit a parallelogram shape in emission (see Fig. 2). This shape, previously seen at lower angular resolution, was interpreted as an S-shape, possibly associated with shocks (Mirabel 1999; Leeuw et al. 2002). A parallelogram morphology has been seen previously in other galaxies. For example, dust absorption features in the SO galaxy NGC 4753 exhibit a parallelogram shape, and have been modeled with a warped twisted disk by Steiman-Cameron et al. (1992). When an optically thin warped disk is seen in emission, the edges of folds in the disk correspond to regions of higher surface brightness. Multiple folds are seen along the line of sight (e.g., Bland 1986; Bland et al. 1987; Quillen et al. 1993; Nicholson et al. 1992) implying that some parts of the disk are seen through other parts of the disk. In this case the morphology would not be nearly symmetric across the origin ( $r \rightarrow -r$ ), as observed, unless the outer disk was nearly optically thin in the mid-infrared. We infer that the disk probably has a low normal optical depth in the mid-infrared (if observed face-on), though the bright edges of the folds and individual clumps in the disk may not be optically thin. The parallelogram is present in all four IRAC bands, though it is most prominent compared to the diffuse emission from

starlight in the longer wavelength  $5.8$  and  $8 \mu\text{m}$  bands.

In visible or near-infrared bands, folds can correspond to regions where the absorption from dust obscures background starlight. In this case folds that are closer to the observer absorb more background starlight from the galaxy. Thus some of the features seen in emission in the IRAC images resemble and coincide with absorption bands previously seen in near-infrared images. In Figure 3 we show a color map made from 2 Micron All Sky Survey (2MASS) images from the 2MASS large galaxy atlas (Jarrett et al. 2003). The south-eastern edge of the parallelogram in the IRAC images lies in the same location as the absorption band  $\sim 10''$  to the south east of the nucleus prominent in the near-infrared images. This is consistent with the study by Leeuw et al. (2002), who compared submillimeter images to near-infrared images. The edge of emission  $\sim 1'$  to the north of the nucleus (at a surface brightness below that of the parallelogram) in the  $8.0 \mu\text{m}$  IRAC image corresponds to the top of the dust lane prominent in optical images of the galaxy. This corresponds to the extinction feature in the near-infrared color map to the north of the nucleus. From comparing the IRAC images to the 2MASS images we infer that the southern side of the parallelogram is closer to the observer than the northern side. Because the dust on this side lies in front of the plane perpendicular to the line of sight containing the galaxy nucleus, it absorbs more background starlight and so causes a deeper band of extinction in the near-infrared images. The northern side of the parallelogram lies on the opposite side and so is not seen in the near-infrared images. Likewise the oval edge of emission  $\sim 1'$  to the north of the galaxy nucleus (see Fig. 2) is nearer the observer than that on the opposite edge  $\sim 1'$  to the south of the nucleus, and only the northern side causes an absorption feature in the near-infrared images and color maps (see Fig. 3).

### 3. MODELING OF THE WARPED DISK

At many observed wavelengths, the morphology of Centaurus A is well reproduced by geometric models of a warped disk (Bland 1986; Bland et al. 1987; Quillen et al. 1992; Nicholson et al. 1992; Quillen et al. 1993; Sparke 1996). We describe and extend such modeling here.

A warped disk can be described as a series of tilted rings, each with a different radius  $r$ . We assume that the gas and dust are evenly distributed on each ring and each ring is smoothly connected to those at larger and smaller radii. We follow the notation and framework used by Quillen et al. (1992, 1993) to describe the geometry of a warped disk. Each ring is described by two angles, a precession angle  $\alpha(r)$  and an inclination angle  $\omega(r)$ . These angles are given with respect to an assumed principal axis of the underlying elliptical galaxy. This axis requires two angles to describe,  $\chi$ , corresponding to the position angle counter clockwise from north of the axis on the sky, and an inclination angle,  $\vartheta$ , that describes the tilt of this galactic axis with respect to the line of sight (see Fig. 6 by Quillen et al. 1993). We assume that the galaxy is axisymmetric and not triaxial so a third angle is not required to describe its orientation. We also assume that the galaxy shape is fixed, and not tumbling.

Our description for the ring projection angles can be related to those of previous works. While Quillen et al.

<sup>1</sup> <http://ssc.spitzer.caltech.edu/archanaly/contributed/browse.html>

<sup>2</sup> <http://ssc.spitzer.caltech.edu/postbcd/>

(1992, 1993) described the angles of the warped disk with respect to the principal axis of the underlying elliptical galaxy, Bland et al. (1987) and Nicholson et al. (1992) matched the  $H\alpha$  velocity field with a tilted ring model describing the orientation of the rings with respect to the line of sight. This model fit the velocity field by adjusting the ring inclination as a function of radius,  $i(r)$ , and position angle counter clockwise from north,  $p(r)$ .

To produce a model image of the mid-infrared emission, we must consider all emitting and absorbing regions along the line of sight at each position on the sky. This is much simpler when the system is optically thin. In this case, we sum all emission along the line of sight at each position on the sky. The near symmetry of the disk suggests that we can use an optically thin approximation to model this disk. While individual clouds could contain optically thick regions, the bulk of the emitted mid-infrared light is likely to reach the observer. When the disk is optically thin, brighter areas correspond to regions that appear folded from the perspective of the viewer. Here we neglect emission from a spherical component associated with the stars and only consider emission from a thin but warped disk.

Our numerical procedure begins by randomly sampling  $x, y$  positions in the plane perpendicular to the principal axis of the elliptical galaxy. At each position we compute a  $z$ -coordinate based on a smooth (spline) function for the disk precession and inclination angles,  $\alpha(r)$  and  $\omega(r)$ . The points that specify these spline functions are listed in Table 1. The coordinates for each point are then rotated into the viewer's frame. Points along each line of sight are summed to produce a model image. For the functions  $\alpha(r)$  and  $\omega(r)$ , we began with those from Quillen et al. (1993) and slightly varied the angles at different radii to achieve a better match to the observed morphology. Matching was done by visual comparison to the IRAC images. No minimizing fit to the image data values was done. Our procedure is adequate to understand the projection affects associated with an emitting warped disk. Future and more intensive modeling would be required to do a multi-dimensional and multi-wavelength fit.

To construct a model, we must consider the thickness of the disk and its brightness distribution. Because the disk is not infinitely thin we randomly chose slight offsets from the  $z$ -coordinate computed from the precession and inclination angles. The size of the offset depends on a disk aspect ratio  $k(r) = h/r$ , where  $h(r)$  is the disk thickness as a function of radius. We assumed for the disk aspect ratio a power law form,  $k(r) = k_{50}(r/50'')^{\beta_z}$ . The intensity of the emission contributed at each point was then computed assuming that the disk volume emissivity integrated through the disk vertically is a power law function of radius,  $\epsilon(r) \propto r^{-\beta_e}$ . We also allowed an inner gap in the radial surface brightness profile,  $r_{gap}$ . The contribution from the active nucleus and the  $\sim 100$  pc circumnuclear disk are not taken into account in our model so by a gap we mean a deficit within  $r_{gap}$  and that of the circumnuclear disk at  $\sim 6''$ .

A model intensity image computed as described above is shown in Figure 4 along with the  $8.0\mu\text{m}$  IRAC image of the galaxy. The numerical parameters of this model are summarized in Table 1. The angle precession and inclination angular functions,  $\alpha(r)$  and  $i(r)$ , are shown in Figure 6 as a solid and dashed lines, respectively. The

precession angle used previously by Quillen et al. (1993) from matching the near-infrared morphology is shown as a dotted line in this figure and is similar to our best matching model. The *Spitzer* data allow us to better study the outer parts of the disk than possible with the old  $^{12}\text{CO}(2-1)$  spectra and near-infrared images. Thus there are some differences in the precession angle  $\alpha(r)$  between our old model and our newer one, as shown in Figure 6. To better match the morphology in the outer parts of the disk we allowed the disk to twist further (to higher a higher value of  $\alpha$ ) before decreasing at larger radius.

Our model predicts that the disk alternates between having the southern side and northern side nearest, with folds both above the nucleus. The near-infrared images show a strong dust absorption feature to the southwest of the nucleus corresponding to an inner fold, and a weaker feature north of the nucleus corresponding to an outer fold (Quillen et al. 1993). In Figure 5 we show the rings comprising our warp model, projected on the sky. The nearer semi-circle of each ring is shown in red, whereas the more distant semi-circle is shown in blue. The disk at  $r \sim 60''$  is nearest the observer on the south-east side. This region corresponds to a fold in the disk that is seen in the near-infrared color map,  $10''$  to the south-east of the nucleus (see Fig. 3). At  $r \gtrsim 100''$  the northern side of the disk is again nearest the observer. This corresponds to the northern dust lane seen in the the optical images and the near-infrared color map about  $45''$  north of the nucleus.

### 3.1. Comparison to previous studies on the geometry of the warped disk

In Figure 7a,b, we show the inclination and position angles as a function of radius with respect to the viewer; functions that can be directly compared to those found by Nicholson et al. (1992) from their kinematic fits to the  $H\alpha$  velocity field (see their Fig. 9a,b). Nicholson et al. (1992) adopted a distance of 3 Mpc to the galaxy, so their linear scale is 15% different than ours; we have corrected for this difference by rescaling the given distances. We see from Figure 7 that the position angles of their tilted ring fit are quite similar to those predicted by our model.

The warp shape originally designed to match the velocity field in molecular gas (Quillen et al. 1992) resembled that which matched the  $H\alpha$  velocity field by Nicholson et al. (1992). Both models included an inclined disk that tilted so that gas rings at different radii alternated between being retrograde and prograde with respect to the observer. This was also a characteristic of the high inclination warp model for NGC 4753 by Steiman-Cameron et al. (1992). The tilted ring fit by Nicholson et al. (1992) to the velocity field did not specify which side of the each ring was closest the viewer. However Bland (1986), Bland et al. (1987), Nicholson et al. (1992), and Quillen et al. (1993) used the visible and near-infrared images to break this degeneracy. The disk is tilted so that it is nearer the viewer on the southern side for intermediate radii; accounting for the southern edge of the dust lane seen in optical images, and nearer the viewer on the northern side at largest radii to account for the northern dust lane seen in the optical and near-infrared images. These flips in orientation can be seen from Figure 7b. They occur where the inclina-

tion with respect to the viewer crosses  $90^\circ$  at which point the disk is edge-on.

The model by Quillen et al. (1993) had a somewhat lower inclination for the galaxy principal axis,  $\vartheta = 65^\circ$ , instead of  $75^\circ$ , used here. Their model also had a higher disk inclination with respect to the galaxy principal axis at smaller radii. There is redundancy in the model between the inclination of the disk with respect to the galaxy axis,  $\omega(r)$ , and the tilt of the galaxy principal axis,  $\vartheta$ . The maximum and minimum ring inclinations correspond to values set by  $\vartheta \pm \omega$  (see discussion by Quillen et al. 1992). To exhibit the parallelogram shape, the disk inclination with respect to the viewer must go above and below  $90^\circ$  causing folds in the disk. This restricts the models to a range of values  $\vartheta + \omega \sim 100^\circ$ .

Here, we find a somewhat better match (see Fig. 8) to the mid-infrared images with a model that has decreasing inclination (with respect to our estimated galaxy principal axis) at larger radii. However this decrease may be spurious. To compute the model at sufficient resolution to compare to the inner region, we cannot well sample points over a large region. By accounting for every observed feature we may have achieved a better morphology match with a model that has exaggerated variations in the ring angles. In other words, the angular variations may have been compressed into a smaller radii than they should be.

To be more certain of the orientation of the outer disk, better kinematic constraints on this outer disk are needed. By specifying a choice for the principal axis of the galaxy, we have chosen to describe the geometry of the warped disk with respect to a particular axis. This choice helped Quillen et al. (1993) compare the shape of the disk to the predictions of simple merger and precessing ring models. However, it is not necessarily significant that the disk inclination as measured with respect to our assumed galaxy axis varies slowly with radius. An additional complexity not considered with our choice of projection angles is that the galaxy may be triaxial, or significantly vary in shape and orientation with radius (e.g., as considered by Arnaboldi & Sparke 1994). The galaxy could be in the process of dynamic relaxation following the merger. Analytical models or one-dimensional integrations fail to capture the complexity of more detailed numerical simulations, particular for near equal mass mergers (e.g., Mihos 1999; Mihos & Hernquist 1996). Imaging and kinematic studies of the outer galaxy suggest that these additional degrees of freedom are important (Malin et al. 1983; Schiminovich et al. 1994; Hui et al. 1995; Peng et al. 2002).

### 3.2. In context with the dynamical warp models

The model precession angle  $\alpha(r)$  reaches a maximum at  $r \sim 100''$ , decreasing at both larger and smaller radii (see Fig. 6). This implies that the corrugated disk is twisted in one direction for  $r \lesssim 100''$  and in the opposite direction for  $r \gtrsim 100''$ . Since the near-infrared morphology depends on which side of each ring is closer to the observer, and our model is similar to that used to match the near-infrared images (also see discussion by Bland et al. 1987; Nicholson et al. 1992), this peculiar change in the handedness of the twist is likely to be real. When the handedness of the twist is the same at all

radii, a nested set of parallelogram shapes can be seen (e.g., as in M84; Quillen & Bower 1999). However in Centaurus A, an outer oval is seen in the outer disk (see Fig. 8 and 5) that is slanted in the opposite direction as the inner parallelogram. This difference in the direction of the slant is a feature of the sign change in the slope of the precession angle.

The precession rate of a gas ring inclined with respect to the underlying galaxy undergoing circular motion is proportional to the ellipticity of the galactic gravitational potential and the angular rotation rate of the ring (e.g., Tubbs 1980; Sparke 1984). If the self gravity of the ring is important then it too can affect the precession rate (Sparke 1986; Arnaboldi & Sparke 1994; Sparke 1996). The direction of precession depends on the orientation of the ring and galaxy (whether a polar ring or not) and whether the galaxy is prolate or oblate. Most models assume that following a merger the gas and dust are distributed in a plane that is misaligned with the principal axes of the galaxy. To be consistent with the direction of the twist in the outer parts of Centaurus A (decreasing  $\alpha(r)$  at  $r \gtrsim 100''$ ), the galaxy can either be prolate and the ring located near the equatorial plane (Quillen et al. 1993) or the galaxy can be oblate and the ring would be nearly polar (Sparke 1996).

The reversal in the sign of the slope ( $d\alpha/dr$ ) is unlikely to be caused solely by the shape of the rotation curve. The predicted rotation curve of Centaurus A increases at smaller radius; all the way to a radius of  $10''$  (see Fig. 13 by Marconi et al. 2005). Consequently the angular rotation rate should increase as the radius decreases nearly all the way to the galaxy center. The rotation curves used by Quillen et al. (1993) and Sparke (1996) were nearly solid-body at small radii, and so underestimated the angular precession rate at small radii (within  $\sim 1.5'$  of the nucleus).

The reversal in the sign of the slope ( $d\alpha/dr$ ) could be due to a drop in the galaxy eccentricity (exploited by both Quillen et al. 1993; Sparke 1996) that would reduce the precession rate at small radii. To account for the change in slope of  $\alpha$  at  $r \sim 100''$ , Quillen et al. (1993) assumed a sharp cutoff in the ellipticity of the gravitational potential of the galaxy as a function of radius. For  $r < 80''$ , the potential ellipticity was much reduced in the model by Quillen et al. (1993) compared to that outside it. The galaxy isophotes are best viewed in the short wavelength  $3.6\mu\text{m}$  IRAC image where the stellar light most contributes to the flux and the extinction and emission from dust is minimized compared to that at shorter wavelengths in the near-infrared. Galaxy isophotal contours for this image are shown in Figure 9.

We first examine the isophotes at  $3.6\mu\text{m}$  to search for evidence of the large scale stellar bar proposed by Mirabel (1999). If such a bar were responsible for the parallelogram shape in the mid-infrared images, the bar would be viewed at intermediate inclinations (not edge-on), and so should be evident in the isophote shapes. However, the isophotes do not exhibit a region of flat surface brightness or a change in ellipticity or position angle over a short range in radius. These features would be expected at the end of a stellar bar. We conclude that there is no evidence for a large scale, few kpc sized, stellar bar at the heart of Centaurus A.

The galaxy isophotal ellipticity does decrease in the

inner regions. By fitting contours to the  $3.6\mu\text{m}$  image outside the emitting disk, we measured a galaxy isophotal ellipticity for the stellar distribution ( $\epsilon = 1 - b/a$ , where  $b$  and  $a$  are the semi-minor and semi-major axes) of  $\epsilon \sim 0.1$  at  $r \sim 4'$ ,  $\epsilon \sim 0.05$  at  $r \sim 2'$ , and  $\epsilon \sim 0$  at  $r < 1'$ . Because the gravitational potential is a convolution of the density profile with a  $1/r$  function, the gravitational potential contours are smoother than the associated density distribution. However, the isophotes are likely to be rounder and smoother than the actual density distribution. While the drop in background galaxy ellipticity exploited by Quillen et al. (1993); Sparke (1996) in their dynamical models is real, it may not be sharp enough to account for the abrupt drop in the precession rate inferred in the central region of the galaxy from the change in the slope of the precession angle  $\alpha$  at  $r \sim 100''$ .

We now consider the role of the mass in the disk. Sparke (1996) showed that the self gravity of the disk could increase the precession rate and vary the precession axis in the central region. Sparke (1996) only considered the mass in the molecular and atomic gas components. Quillen et al. (1993) noted that there were extensions in the K-band isophotes that were not reproduced by the purely absorptive disk model. The K-band isophotes are extended at a radius of about  $60''$  in the  $15\text{ mag/arcsec}^2$  contour (also see the dereddened contour map shown in Figure 9 by Marconi et al. 2005). We can compare the mass in a possible disk gas and stellar component to that in the underlying galaxy. With a circular rotational velocity of  $250\text{ km s}^{-1}$ , a total mass of  $\sim 10^{10} M_\odot$  is enclosed within a radius of 1 kpc. The mass in molecular gas in the same region is a few times  $10^8 M_\odot$  (Phillips et al. 1987, corrected for the difference in the assumed distance). The level of  $15\text{ mag arcsec}^{-2}$  in K-band corresponds to a surface density of  $4500 M_\odot \text{ pc}^{-2}$  assuming a mass to light ratio at K-band of 0.5 (e.g., Silge et al. 2005). The actual surface density would be  $\sim 10$  times lower than this, taking into account the mean disk axis ratio on the sky. This surface density can be compared to the estimated surface density of molecular gas, or a few hundred  $M_\odot \text{ pc}^{-2}$ . This suggests that at least an equal mass exists in stars in the disk as in gas.

Comparing the total mass in gas and stars in the disk to that in the underlying spherical component, we estimate that a few percent of the total mass within 1 kpc lies in the disk. The mass in the disk is likely to be a few times larger than that used by Sparke (1996) to account for the disk geometry. We support the finding by Sparke (1996) that the self-gravity in the disk is important, and so should significantly affect the disk precession rate. Future modifications of the prolate model should take this into account, as the self-gravity in the disk could change the direction of precession in this region. If the outer disk is prolate, then a reversal in the twist could be due to the self-gravity of the disk in the inner region. If the outer galaxy is oblate, then the ring is polar and the model by Sparke (1996) would account for the reversal in the twist of the disk. Both dynamical models could be updated to include better estimates of the mass in the disk, the galaxy isophotes at  $2.2$  and  $3.6\mu\text{m}$ , and an improved rotation curve based on the light distribution.

### 3.3. A gap in the dusty disk between a radius of $6''$ and $50''$

The model that is most similar to the IRAC images (shown in Fig. 4) contains a gap in the dust distribution with outer radius  $r \sim 50''$ . We compare the model shown in Figure 4 to a similar one that lacks the deficit in the dust distribution. This model is shown in Figure 10a, and does not match the observed morphology as well as that containing a gap in the dust distribution. The smooth continuation of the precession angle into the inner region results in an edge-on disk with respect to the viewer at some point within  $r = 60''$ . This causes the sharp bright linear feature at  $r < 60''$  seen in Figure 10a that is not exhibited by the IRAC images.

If the disk has a lower inclination with respect to the viewer, the observed surface brightness is reduced. We consider the possibility that the disk precession angle differs in the inner region from that expected from a smooth continuation of our model. To test this possibility, we computed a model that has a flattened (non-twisted) disk at  $r \lesssim 60''$ . This model is shown in Figure 10b. The sharp, bright, inner feature along the east-west direction seen in Figure 10a is not evident in Figure 10b. However, the morphology of this model also does not display the characteristics of our preferred model shown in Figure 4 that better resembles the IRAC images. In particular, the triangular features to the south-east and north-west of the nucleus that are seen in the near-infrared color maps on the south-east side (Quillen et al. 1993) are not as good a match to those of the IRAC images. To remove the bright inner feature of Figure 10a, the precession angle must remain above  $\alpha > 270^\circ$ . However, the curved triangle edge of emission in the parallelogram is not present if the precession angle does not steeply drop between a radius of  $100''$  and  $50''$ . We have tried models with both increasing and decreasing precession angles near the nucleus, finding no improved match to the observed morphology. Our best match is the model with an inner gap in the dust distribution. We explored models with a lower but constant surface density within the estimated gap radius of  $\sim 50''$ , and can exclude those with a surface density in the gap that is above  $1/5$  of that at the outer gap edge.

Previous studies have discussed the possibility of a deficit in the gas distribution in the same region as we find a deficit in the dust distribution. At  $100\text{--}200\text{ pc}$  from the nucleus there is a circumnuclear molecular disk that has been studied in molecular line emission (Israel et al. 1990, 1991). A deficit in the ionized gas distribution outside the circumnuclear disk was seen in the  $\text{Pa}\alpha$  kinematics by Marconi et al. (2001). In  $\text{Pa}\alpha$ , the circumnuclear disk at a radius of  $r \sim 6''$  is seen, and so is emission at significantly lower velocities (hence inferred larger radii) and significantly higher velocities (within the sphere of influence of the massive black hole). However  $\text{Pa}\alpha$  emission is lacking at intermediate radii and velocities. This lack of emission would be expected if there were a deficit of gaseous material between the radii of  $\sim 6''$  (set by the estimated outer radius of the circumnuclear disk, Schreier et al. 1996; Marconi et al. 2000, 2001) and  $50''$  (estimated from our model).

The rotation curve previously fit to the CO and  $\text{H}\alpha$  kinematics rose linearly (solid body) within a radius of  $1'$  of the nucleus (Quillen et al. 1992; Nicholson et al. 1992). Because an edge-on gas ring appears linear on a position-velocity diagram, a gas disk with an inner hole

can mimic or be confused with a gas disk extending all the way to the nucleus in a galaxy with a linearly rising rotation curve. Nicholson et al. (1992) showed that there was a discrepancy between their measured rotation curve and that expected from a  $r^{1/4}$  or deVaucoulers law. They listed a possible hole in the HII region distribution as a possible cause for this discrepancy. A linearly rising rotation curve within a radius of  $1'$  of the nucleus is not consistent with the K-band surface brightness profile (see the rotation curve predicted in Figure 13 by Marconi et al. 2005). The apparent region of solid body rotation need not be accounted for with a galactic bar, as proposed by Mirabel (1999), and can be better explained by a gap in the gas and dust distribution.

#### 4. SUMMARY AND DISCUSSION

By integrating the light through an emitting, optically thin, dusty, and warped disk, we have successfully matched the morphology of Centaurus A seen in mid-infrared IRAC images. We confirm previous proposals that the disk morphology is well explained by a warped disk (Bland 1986; Bland et al. 1987; Quillen et al. 1993; Nicholson et al. 1992; Leeuw et al. 2002) rather than a barred one (Mirabel 1999). The disk is nearly edge-on with respect to the viewer, but tilts so that folds appear above and below the galaxy equator. There is a fold south of the nucleus at a radius  $r \sim 60''$  responsible for high extinction seen in near-infrared images, and a fold north of the nucleus at larger radii responsible for the northern edge of the dust lane seen in optical and images. Extinction features seen in the near-infrared extinction map correspond to folds in the disk that are located nearer the observer and so absorb more background stellar light from the galaxy. In the mid infrared, however, folds on both the near and opposite side of the galaxy correspond to bright emission features. The inner folds account for the parallelogram shape, while the outer folds account for the northern edge of the dust lane seen in optical images and a fainter oval of emission seen outside the parallelogram in the IRAC images.

The disk geometry we use to match the mid-infrared morphology is similar to that found previously by Quillen et al. (1993), and is also similar to that required to fit the CO and  $H\alpha$  velocity field (Bland et al. 1987; Quillen et al. 1992; Nicholson et al. 1992). The geometric warp models by Quillen et al. (1993); Nicholson et al. (1992) have been predictive; they provide good matches to the mid-infrared morphology. Some differences in the precession angle exist in the model at  $r \gtrsim 100''$  compared to previous work. Previous CO,  $H\alpha$  spectra and near-infrared imaging were not sensitive enough to provide tight kinematic constraints on the outer disk. The *Spitzer* data have allowed us to extend the model past  $r \sim 100''$  compared to previous models and see closer in to the nucleus where the extinction is high at shorter wavelengths. Better constraints on the disk geometry could be achieved in the future by fitting observations at more than one wavelength. For example, modern high resolution kinematic observations that are fit along with the *Spitzer* data using the same model would allow much stronger constraints on the disk geometry and gas and dust distribution than the slight modification to previous geometric models that we have used here.

The warp disk model suggests that there is a gap in

the dusty disk at  $6'' \lesssim r \lesssim 50''$ . A gap exists in same region in the gas distribution. Marconi et al. (2001) saw a deficit of  $Pa\alpha$  emission near the nucleus at intermediate velocities. Nicholson et al. (1992) suggested that the discrepancy between the measured linearly rising rotation curve within a radius of  $60''$  might be explained by a hole in the ionized gas distribution. It is not easy to determine if there is a gap in the dust distribution since the infrared surface brightness depends on the inclination of the disk and the disk is highly corrugated. If the disk twists to lower inclinations (closer to face-on) at small radii, it would have a lower surface brightness near the nucleus. We have explored models with smoothly varying radial surface brightness distributions, and smoothly varying precession and inclination angles. We find that only models with a deficit of dust interior to  $\sim 50''$  resemble the mid-infrared images. We exclude models that have more than  $\sim 1/5$  the surface density within  $r = 50''$  as at that radius. We conclude that there is a gap in the gas and dust distribution between 0.1 and 0.8 kpc from the nucleus. The inner radius of the gap we have taken from studies of the circumnuclear disk (Marconi et al. 2001; Israel et al. 1991), and the outer radius is estimated from our model.

It is interesting that only the region between the circumnuclear disk (100–200 pc) and  $\sim 0.8$  kpc has been depleted of gas and dust. While we find no evidence for a large scale stellar bar in Centaurus A, a dense gas disk could have exhibited dynamical instabilities depositing gas into the circumnuclear disk (e.g., Shlosman et al. 1989). Energetic star formation or activity associated with the black hole can deplete and evacuate the central region of a galaxy (e.g., Springel et al. 2005; Veilleux et al. 2005), though it is not clear how a circumnuclear disk would be protected from or reformed following this activity. Nearby galaxies exhibit evacuated central regions or circumnuclear rings. For example, the Circinus galaxy has a  $\sim 500$  pc radius molecular ring (Curran et al. 1998) and contains a Seyfert nucleus. M82 contains a 1 kpc radius circumnuclear molecular ring; however, a previous epoch of star formation has occurred within this ring (e.g., Forster Schreiber et al. 2003). Future observational studies may differentiate between the role of star formation, dynamical instabilities and nuclear activity in disrupting the gas and dusty disk in Centaurus A.

The best matching geometric warp model requires a change in the slope of the precession angle at a radius of about  $r \sim 100''$ . Two previous models account for this twist. Quillen et al. (1993) used a model in which the galaxy was prolate in its outer region and the galaxy ellipticity abruptly dropped to zero within  $r \sim 80''$ . However, this abrupt drop is not consistent with the isophote shapes at  $3.6\mu\text{m}$ . A prolate model (with the advantage of a relatively short timescale) might account for the disk geometry if modified to include the self-gravity of the disk. The polar ring model by Sparke (1996) naturally accounts for the reversal, but requires a longer timescale to operate. These dynamical models could be updated to use a more accurate mass distribution and rotation curve. Improvements to these models may lead to better understanding of the galaxy merger that created Centaurus A's peculiar morphology, as well as the merger's role in feeding the active galactic nucleus.

We thank Joss Bland-Hawthorn, Varoujan Gorjian and Vassilis Charmandaris for helpful comments and suggestions. We thank the Research School of Astronomy and Astrophysics of the Australian National University and Mount Stromlo Observatory for hospitality and support for ACQ during Spring 2005. Support for this

work was in part provided by National Science Foundation grant AST-0406823, and the National Aeronautics and Space Administration under Grant NNG04GM12G issued through the Origins of Solar Systems Program. We acknowledge support by award HST-GO-10173-09.A through the Space Telescope Science Institute.

## REFERENCES

Arnaboldi, M. & Sparke, L. S. 1994, AJ, 107, 958  
 Baade, W., & Minkowski, R. 1954, ApJ, 119, 215  
 Bland, J. 1986, Ph.D. thesis, Univ. Sussex  
 Bland, J., Taylor, K., & Atherton, P. D. 1987, MNRAS, 228, 595  
 Charmandaris, V., Combes, F., & van der Hulst, J. M. 2000, A&A, 356, L1  
 Curran, S. J., Johansson, L. E. B., Rydbeck, G., & Booth, R. S. 1998, A&A, 338, 863  
 Fazio, G. G. et al. 2004, ApJS, 154, 10  
 Forster Schreiber, N. M., Genzel, R., Lutz, D., & Sternberg, A. 2003, ApJ, 599, 193  
 Haynes, R. F., Cannon, R. D., & Ekers R. D. 1983, Proc ASA, 5, 241  
 Hernquist, L., & Quinn, P. J. 1988, ApJ, 331, 682  
 Hui, X., Ford, H.C., Freeman, K.C., Dopita, M.A. 1995, ApJ, 449, 592  
 Israel, F. P. 1998, A&ARv, 8, 237  
 molecular disk  
 Israel, F. P., van Dishoeck, E. F., Baas, F., Koornneef, J., Black, J. H., & de Graauw, T. 1990, A&A, 227, 342  
 Centaurus A - Probing the circumnuclear disk  
 Israel, F. P., van Dishoeck, E. F., Baas, F., de Graauw, T., & Phillips, T. G. 1991, A&A, 245, L13  
 Jarrett, T. H., Chester, T., Cutri, R., Schneider, S. E. & Huchra, J. P. 2003, AJ, 125, 525  
 Leeuw, L. L., Hawarden, T. G., Matthews, H. E., Robson, E. I., & Eckart, A. 2002, ApJ, 565, L131  
 Mirabel, I. F., et al. 1999, A&A, 341, 667  
 Malin, D. F., Quinn, P. J., & Graham, J. A. 1983, ApJ, 272, 5  
 Marconi, A., Schreier, E. J., Koekemoer, A., Capetti, A., Axon, D., Macchetto, D., & Caon, N. 2000, ApJ, 528, 276  
 Marconi, A., Capetti, A., Axon, D. J., Koekemoer, A., Macchetto, D., & Schreier, E. J. 2001, ApJ, 549, 915  
 Marconi, A., Pastorini, G., Pacini, F., Axon, D.J., Capetti, A., Macchetto, D., Koekemoer, A.M., & Schreier, E.J. 2006, ApJ, in press, astroph-0507435  
 Mihos, C. 1999, Ap&SS, 266, 195  
 Mihos, J. C., & Hernquist, L. 1996, ApJ, 464, 641  
 Nicholson, R. A., Bland-Hawthorn, J., & Taylor, K. 1992, ApJ, 387, 503  
 Peng, E. W., Ford, H. C., Freeman, K. C., & White, R. L. 2002, AJ, 124, 3144  
 Phillips, T. G., Ellison, B. N., Keene, J. B., Leighton, R. B., Howard, R. J., Masson, C. R., Sanders, D. B., Veidt, B., & Young, K. 1987, ApJ, 322, L73  
 Quillen, A. C., Graham, J. R., & Frogel, J. A. 1993, ApJ, 412, 550  
 Quillen, A. C., de Zeeuw, P. T., Phinney, E. S., & Phillips, T. G. 1992, ApJ, 391, 121  
 Quillen, A. C., & Bower, Gary A. 1999, ApJ, 522, 718  
 (Centaurus A)  
 Schiminovich, D., van Gorkom, J. H., van der Hulst, J. M., & Kasow, S. 1994, ApJ, 423, L101  
 Schreier, E. J., Capetti, A., Macchetto, F., Sparks, W. B., & Ford, H. J. 1996, ApJ, 459, 535  
 Shlosman, I., Frank, J., & Begelman, M. C. 1989, Nature, 338, 45  
 Silge, J.D., Gebhardt, K., Bergmann, M., & Richstone, D. 2005, AJ, 130, 406  
 Sparke, L. S. 1984, MNRAS, 211, 911  
 Sparke, L. S. 1986, MNRAS, 219, 657  
 Sparke, L. S. 1996, ApJ, 473, 810  
 Springel, V., Di Matteo, T., & Hernquist, L. 2005, MNRAS, 361, 776  
 Steiman-Cameron, T. Y., Kormendy, J., Durisen, R. H. 1992, AJ, 104, 1339  
 Tubbs, A. D. 1980, ApJ, 241, 969  
 Veilleux, S., Cecil, G., & Bland-Hawthorn, J. 2005, ARA&A, 43, 769

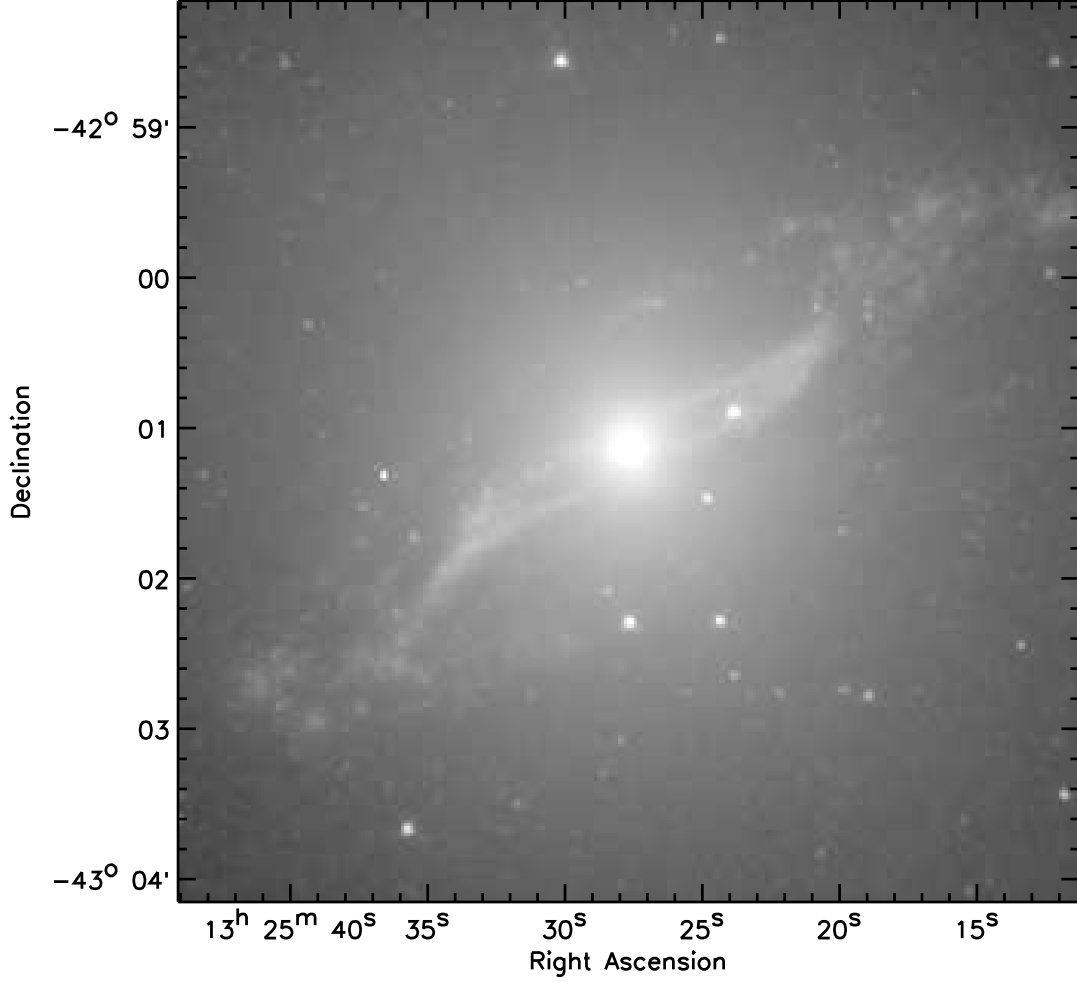


FIG. 1.— a) The central region of the image at  $3.6\mu\text{m}$  taken by the IRAC camera on board the Spitzer Space Telescope. The emission is shown on a log scale. At  $3.6$  and  $4.5\mu\text{m}$  starlight peaking near the galaxy center is seen in addition to emission from dust. At longer wavelengths emission from dust is primarily seen.

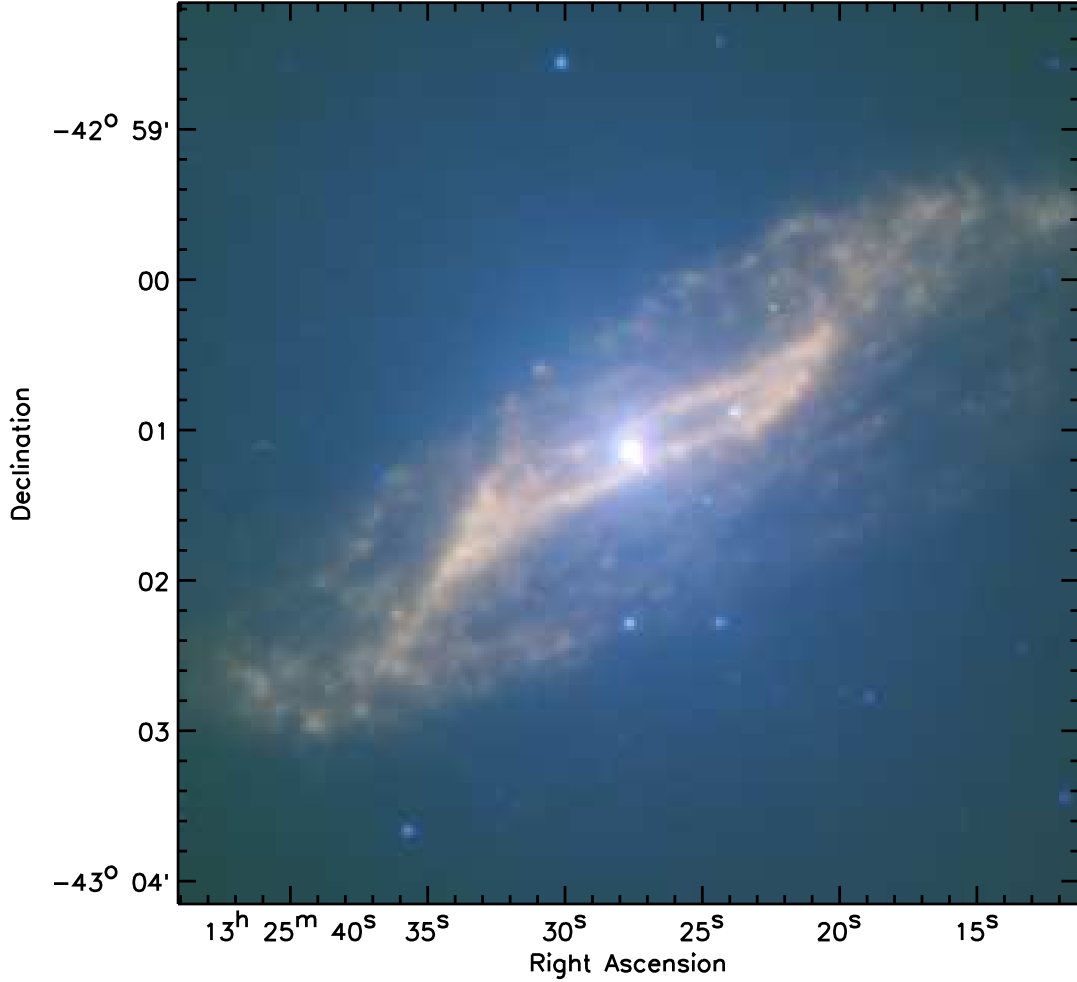


FIG. 2.— The same region as Fig. 1 but a color composite of the IRAC images at 3.6, 5.8 and 8.0 $\mu$ m. This figure is shown on a log scale. The black and white version of this figure only shows the emission at at 8.0 $\mu$ m.

TABLE 1  
MODEL PARAMETERS

Description	Parameter	Value
Galaxy principal axis		
$PA$ on sky	$\chi$	20°
Tilt	$\vartheta$	75°
Dust intensity		
Dust emissivity index	$\beta_e$	4.0
Aspect ratio	$k_{50}$	0.1
Aspect ratio index	$\beta_k$	0.9
Radius of inner hole	$r_{gap}$	50''

NOTE. — The precession angle for this model,  $\alpha(r)$ , is a spline function that interpolates between 10 points in the format (radius in arcseconds,  $\alpha$  in degrees): (0.2, 180), (36.0, 210), (57, 270), (80, 345), (89, 375), (100, 400), (135, 380), (155, 345), (240, 280), (400, 240). The inclination angle  $\omega(r)$  is a spline function that interpolates between the following points (0.2, 25), (100, 20), (260, 8), (400, 8).

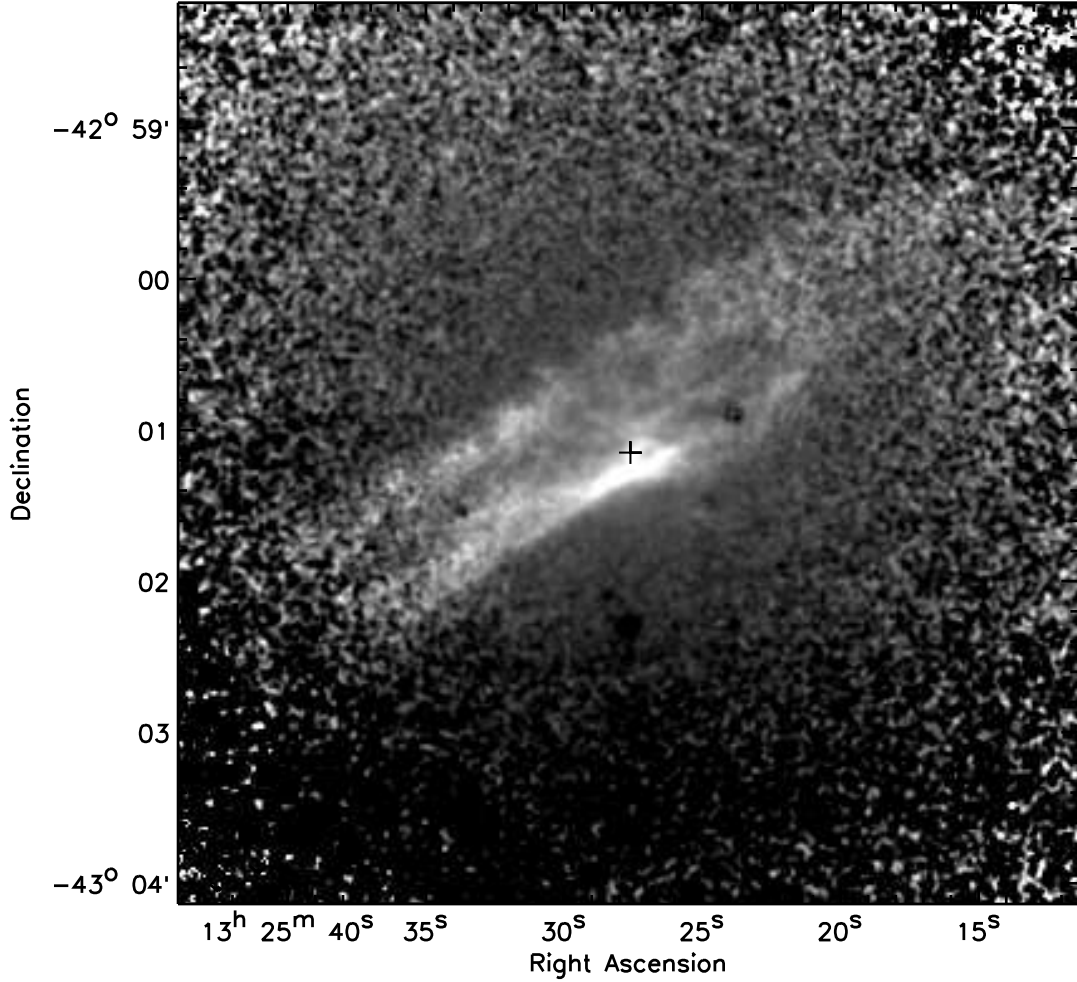


FIG. 3.— Color map showing the log of the H-band divided by the J-band 2MASS images by Jarrett et al. (2003). Lighter shading corresponds to regions of heavier extinction. Folds in the disk both nearer and more distant the observer are seen in the mid-infrared images. However folds nearer the observer absorb more background starlight and so are more prominent in the near-infrared images.

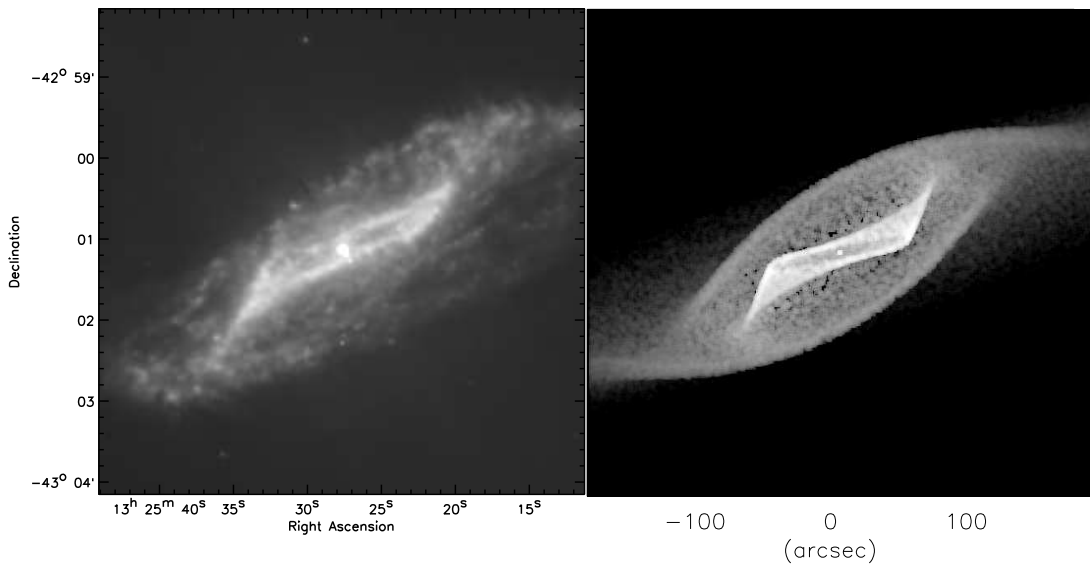


FIG. 4.— On the left is the IRAC 8.0  $\mu$ m image. On the right is the model for the warped disk with parameters given in Table 1.

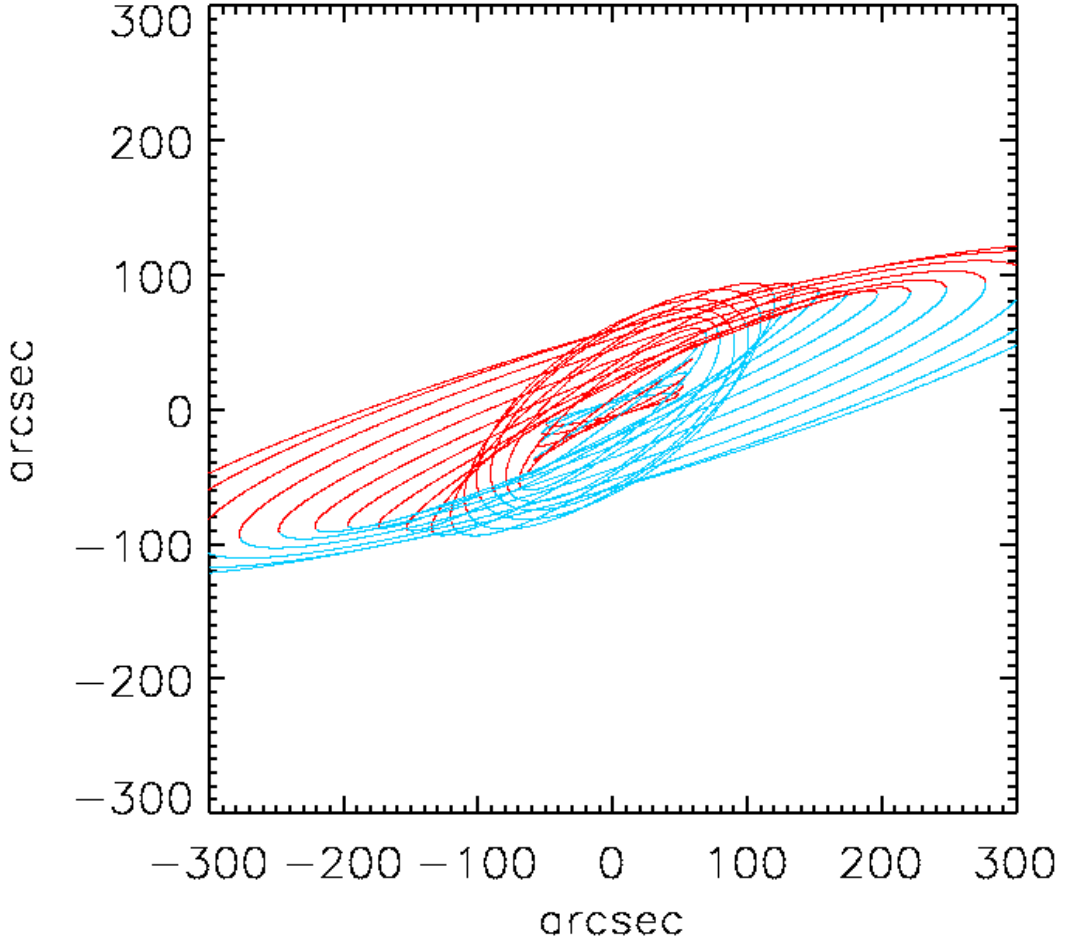


FIG. 5.— This image shows rings for the warped disk model shown in the previous figure. The semi-circle of each ring nearest the observer is shown in red, that more distant shown in blue. *For the black-white version of this figure: The semi-circle of each ring nearest the observer is shown in black, that more distant shown in gray.* At near-infrared and visible wavelengths dust nearer the observer absorbs more background galactic starlight than dust more distant from the observer. The inner fold corresponds to the extinction feature southeast of the nucleus seen in the J/H-band color map (see Fig.3b). The outer fold seen here corresponds to the extinction feature north of the nucleus that is the northern edge of the dustlane prominent in visible images of the galaxy. Regions where rings are close together correspond to regions of higher surface brightness in the mid-infrared images. Though the nearer side can cause deeper extinction features in the near-infrared images, both sides of the disk cause emission features in the mid-infrared images.

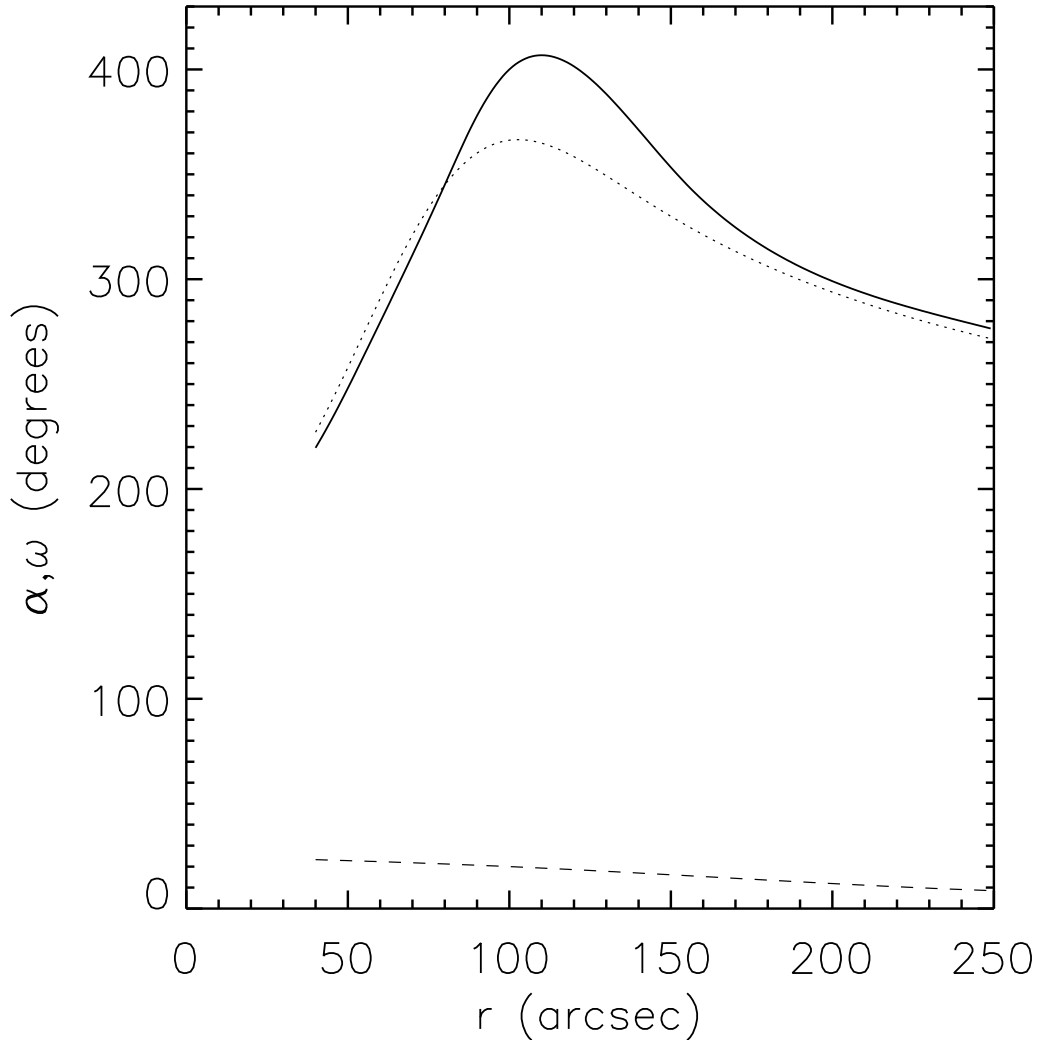


FIG. 6.— The solid line shows the precession angle,  $\alpha(r)$  as a function of radius used to make the model shown in Figure 4. The dashed line shows the adopted inclination angle. For comparison we show as a dotted line the precession angle used for the previous model by Quillen et al. (1993) (based on the near-infrared imaging). These models should be approximately consistent with the CO velocity field by Quillen et al. (1992) and H  $\alpha$  velocity field by Nicholson et al. (1992).

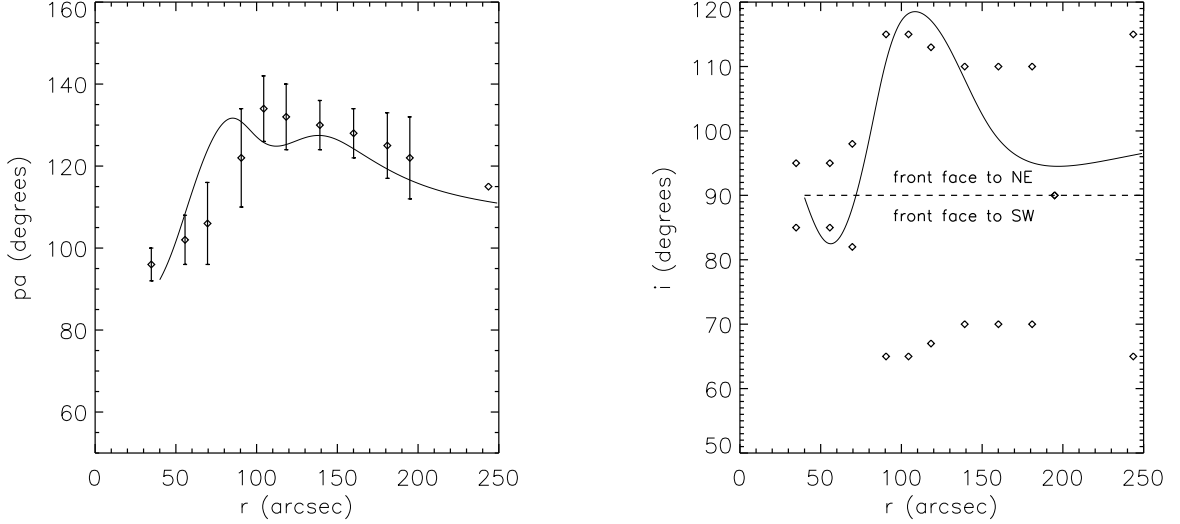


FIG. 7.— a) The position angle of each ring on the sky (anti-clockwise from North) is shown. These angles are compared with those estimated from tilted ring fits from the H $\alpha$  velocity field by Nicholson et al. (1992) that are shown as diamonds. These points were taken from their Figure 9a. b) We show the inclination angle of each ring with respect to the viewer for the model shown in the previous figures. The inclination of an edge-on disk is shown as a dotted line at 90°. Rings with inclinations above 90° are oriented with their nearest points to the north-east of the nucleus, and those with inclinations below 90° have nearest points to the south-west of the nucleus. These angles are also compared with those from the H $\alpha$  velocity field (diamonds). Bland et al. (1987); Nicholson et al. (1992) inferred that at  $r \lesssim 60''$  the front face of the disk is oriented to the south-west of the nucleus, and vice versa for  $r \gtrsim 60''$  (also see Sparke 1996).

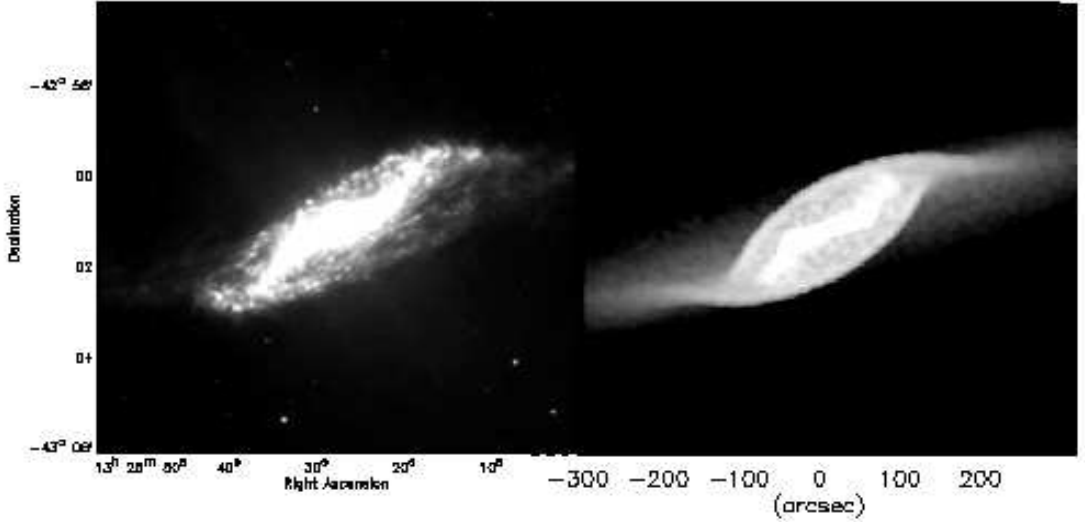


FIG. 8.— Similar to Figure 4 except shown on a larger scale.

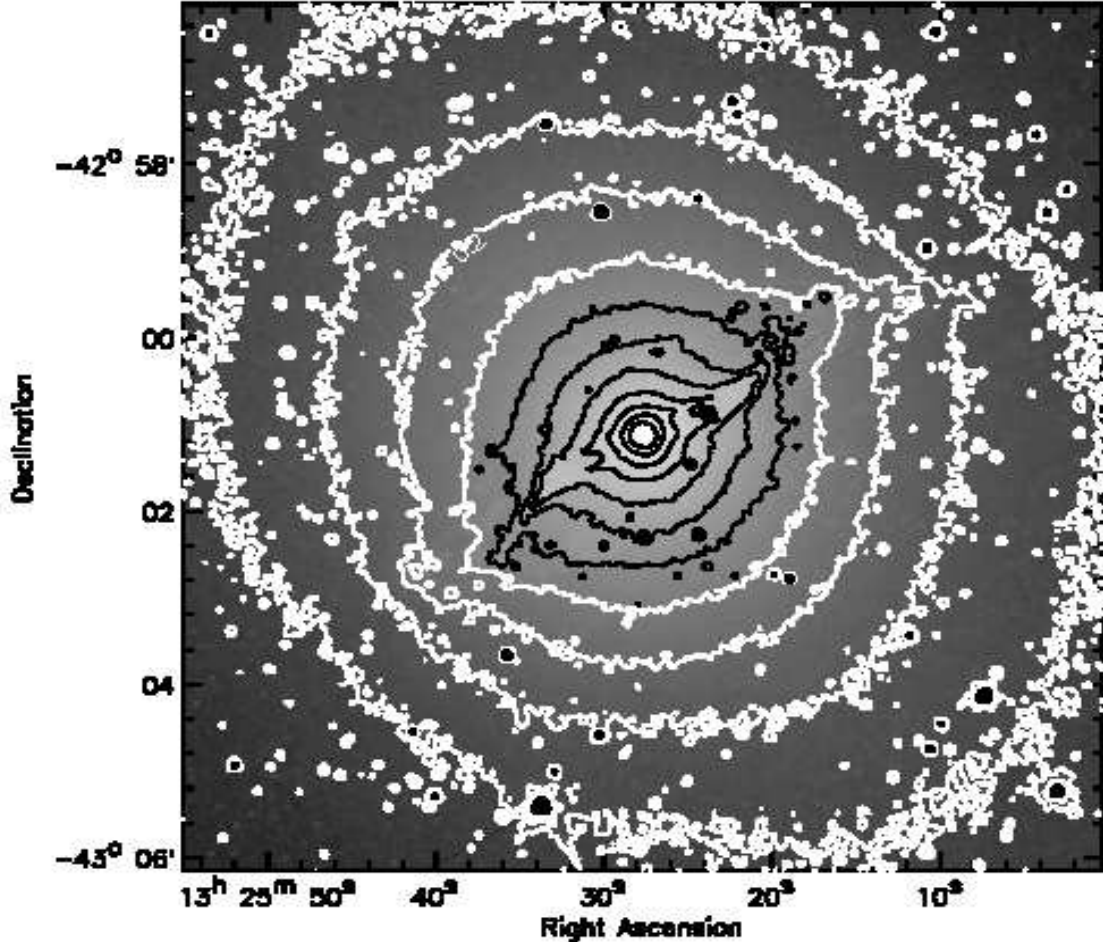


FIG. 9.— The IRAC Band 1 ( $3.6\mu\text{m}$ ) image shown with isophotal contours. The lowest contour is at  $0.63 \text{ MJy sr}^{-1}$ . The contours are separated by 0.5 magnitudes or a factor of 1.585. The galaxy is more highly elliptical at larger radii.

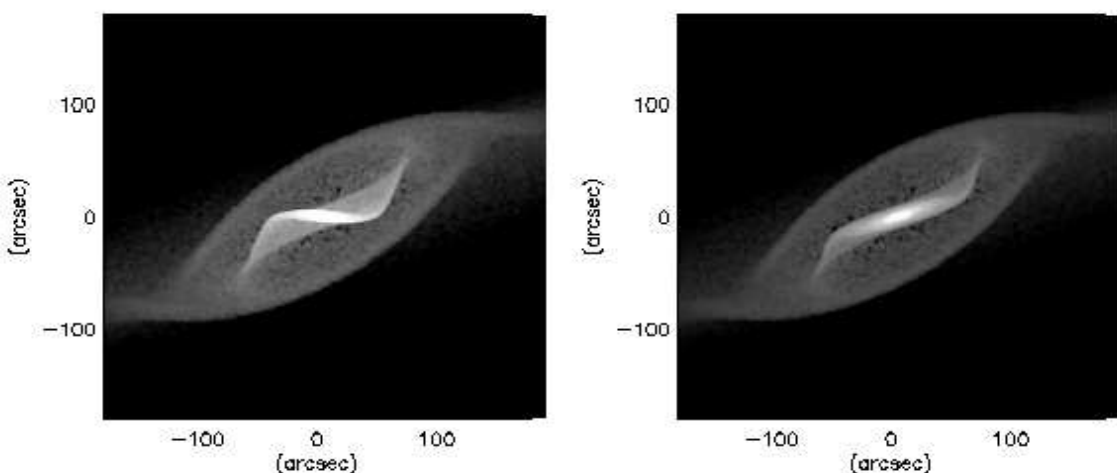


FIG. 10.— a) This model is similar to that shown in Figure 4 except there is no deficit in the dust distribution within  $r_{\text{gap}}$ . b) This model is similar to that shown in Figure 4 except the precession angle  $\alpha(r)$  remains above  $270^\circ$  for  $r < 50''$ . The IRAC images are best matched with a model that contains a deficit in the dust distribution within  $r \sim 50''$ .